Supplemental Table S1

Table S1. Primer information

For genotyping		5' ->3'
Pcgf3	P1	ATAAGATGAGATGGGATGGGC
	P2	ACGCCTCCAGGTGATCCATAC
Pcgf5	P1	TGTTTACAGAGAGGAAGCGCC
	P2	TGGCCTTGGTACACATATAGC

For ChIP-qPCR		5' ->3'
Meis1	Previously described in Yakushiji-Kaminatsui et al., 2016	
Meis2		
Hoxa11 promoter	Forward	CTCGCACCTTGTACCCTGAT
	Reverse	GATGCCGATTGCGTTTAGTT
Hoxa13 promoter	Forward	TCCTGGAACCAACAGGAAAC
	Reverse	TGGCATGTTTTAGGGACCTC
Pitx2 promoter	Forward	ATTTCTCCAGGAGCCATTTG
	Reverse	ACTCTCTGTCGTCGGGAGTC

Supplemental Table S2

Table S2. Public ChIP-seq datasets used in this research

Dataset	Accession number	Reference
E11.5, forelimb proximal, RING1B	GSM1716759	Yakushiji-Kaminatsui et al., RING1 proteins contribute to early proximal-distal specification of the forelimb bud by restricting Meis2 expression, **2016** Development 143, 276-285.
E11.5, forelimb distal, RING1B	GSM1716760	
MV-4-11, Vehicle 1, RARA WCE	SRX2705416	McKeown et al., Superenhancer Analysis Defines Novel Epigenomic Subtypes of Non-APL AML, Including an RARα Dependency Targetable by SY-1425, a Potent and Selective RARα Agonist, **2017** Cancer Discov. 10, 1136-1153.
MV-4-11, Vehicle 2, RARA WCE	SRX2705415	
MV-4-11, Vehicle 1, RARA IP	SRX2705441	
MV-4-11, Vehicle 2, RARA IP	SRX2705440	
MV-4-11, Treated 1, RARA WCE	SRX2705418	
MV-4-11, Treated 2, RARA WCE	SRX2705417	
MV-4-11, Treated 1, RARA IP	SRX2705443	
MV-4-11, Treated 2, RARA IP	SRX2705442	
MV-4-11, Vehicle 1, H3K27ac WCE	SRX2705477	
MV-4-11, Vehicle 2, H3K27ac WCE	SRX2705476	
MV-4-11, Vehicle 3, H3K27ac WCE	SRX2705474	
MV-4-11, Vehicle 1, H3K27ac IP	SRX2705454	
MV-4-11, Vehicle 2, H3K27ac IP	SRX2705453	
MV-4-11, Vehicle 3, H3K27ac IP	SRX2705450	
MV-4-11, Treated 2, H3K27ac WCE	SRX2705478	
MV-4-11, Treated 3, H3K27ac WCE	SRX2705475	
MV-4-11, Treated 2, H3K27ac IP	SRX2705455	
MV-4-11, Treated 3, H3K27ac IP	SRX2705452	
MV-4-11, Treated 4, H3K27ac IP	SRX2705451	

Supplemental Figures

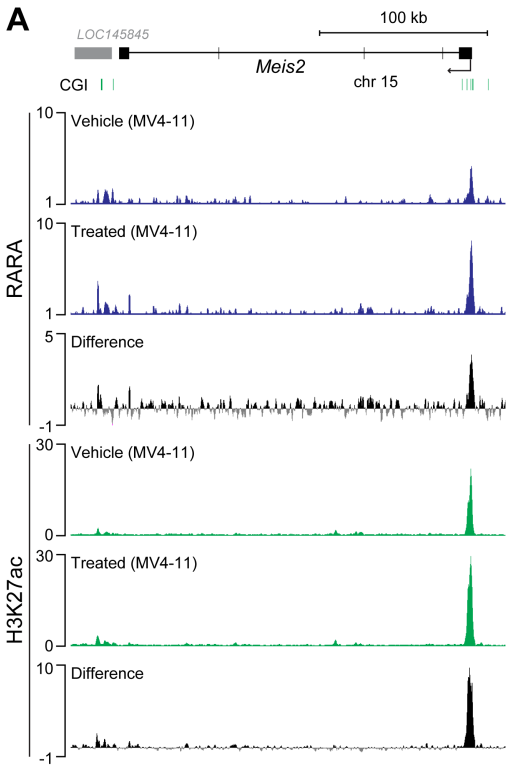

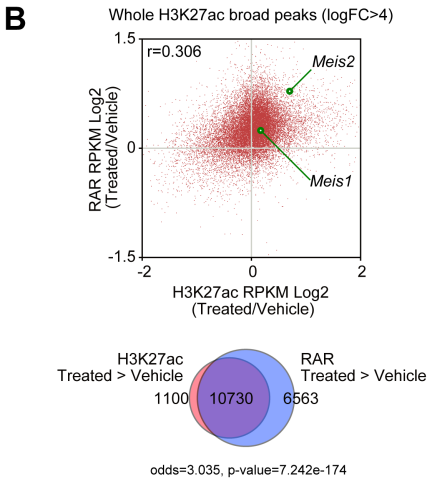

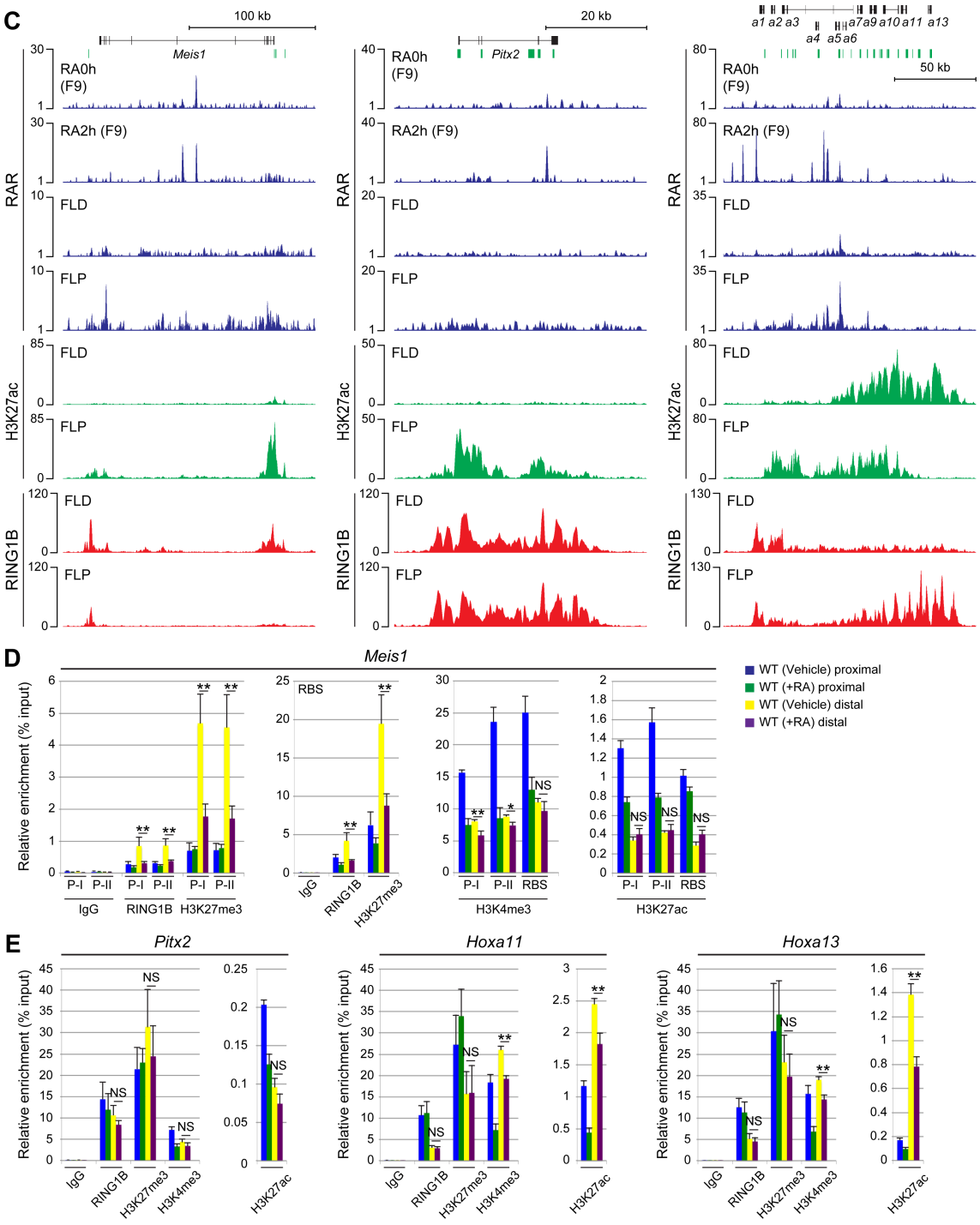

Fig. S1 (related to Fig. 1). Effects of either SY-1425 (tamibarotene) or ATRA on RARα, histone modification and RING1B activities in human MV4-11 cells or mouse forelimb buds at E10.5.

(A) ChIP-seq showing the level of RARA and H3K27ac at *Meis2* locus in MV4-11 cells treated with vehicle or SY-1425, a selective RARα agonist (treated). The difference in the normalized number of reads between the vehicle- and SY1425-treated is shown by negative (gray) and positive (black), respectively (tracks 3 and 6). (B) Scatter plots representing the logarithmic ratio of normalized read counts between SY-1524 stimulated and vehicle-treated MV4-11 cells (top). The alterations in enrichments of H3K27ac and RAR by SY-1425 treatment showed a positive correlation. Overlaps between peaks of RAR and H3K27ac that had significantly enriched and at least more than 2 times reads as compared with whole cell extract (bottom). (C) Distribution of RAR, H3K27ac and RING1B at the *Meis1* (left), *Pitx2* (middle) and *HoxA* (right) locus in F9 cells (0 hour with only vehicle (RA0h)) and 2 hours after RA stimulation (RA2h), E11.5 proximal (FLP) and distal (FLD) forelimb buds revealed by ChIP-seq analysis. (D, E) ChIP-qPCR analysis showing the levels of RING1B, H3K27me3, H3K4me3 and H3K27ac at the TSS and RBS of the *Meis1* (D) and the promoters of *Hoxa11*, *Hoxa13* and *Pitx2* (E) in the proximal and distal regions of E10.5 forelimb buds from wild type (vehicle) and ATRA-treated wild type (+RA) embryos. Error bars indicate s.e.m. of two or three biological replicates. **P<0.01, *P<0.05, NS>0.05, Student's *t*-test. Enrichment of ChIP-seq (*Y*-axis) in (A) and (C) is shown as the normalized depth of coverage.

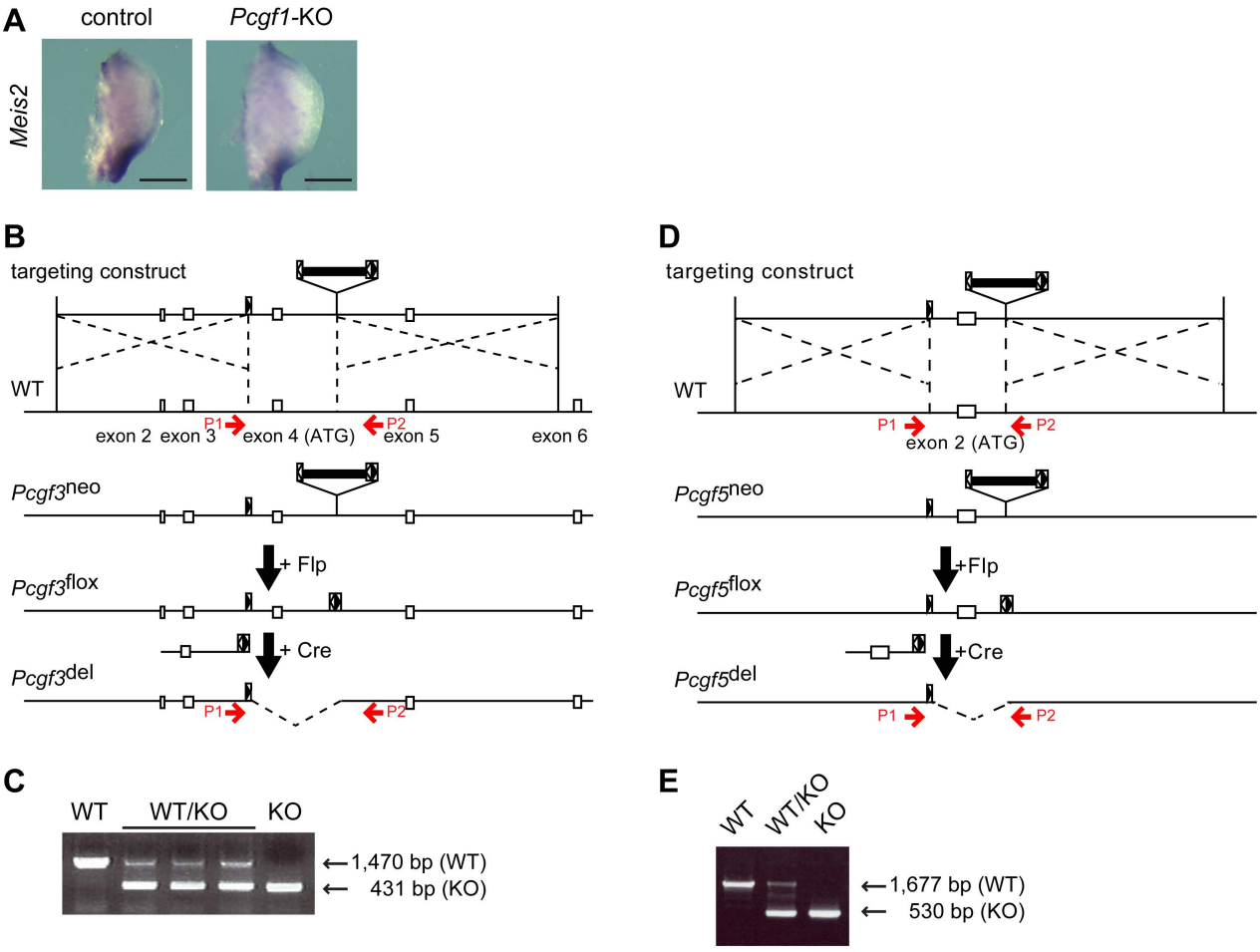

Fig. S2 (related to Fig. 3). *Meis2* expression in *Pcgf1*-KO forelimb buds and Generation of *Pcgf3/5* mutants. (A) *Meis2* expression in control (*Pcgf1*$^{fl/fl}$) and *Pcgf1*-KO forelimb buds at E10.5. Scale bar, 250 µm. (B) Schematic representation of gene targeting strategy to delete *Pcgf3*. Targeting construct to generate the *Pcgf3*^{neo} allele harbors a Neomycin resistant gene cassette (indicated by bold bars), two loxP sites (indicated by closed triangles) and two FRT (open triangles) sites. The Neomycin resistant gene cassette was removed by mating *Pcgf3*$^{neo/+}$ with FLP deleter line (CAG-FLP) to generate the *Pcgf3*^{flox} allele. The *Pcgf3*-KO allele was generated by deleting the 4th exon of *Pcgf3* by crossing mice carrying *Pcgf3*^{flox} with CAG-Cre mouse strain. The *Pcgf3* mutant line was maintained as heterozygotes and KO mice were obtained by mating *Pcgf3*$^{+/-}$ female with *Pcgf3*$^{+/-}$ male. Genomic positions of PCR primers (P1 and

P2) used for genotyping are indicated by red arrows. (C) PCR analysis to distinguish the wild type (WT), *Pcgf3*$^{+/-}$ (WT/KO) and *Pcgf3*$^{-/-}$ (KO). (D) Schematic representation of gene targeting strategy to delete *Pcgf5*. Targeting construct to generate the *Pcgf5*^{neo} allele harbors a Neomycin resistant gene cassette (indicated by bold bars), two loxP sites (indicated by closed triangles) and two FRT (open triangles) sites. The Neomycin resistant gene cassette was removed by mating *Pcgf5*$^{neo/+}$ with FLP deleter line (CAG-FLP) to generate the *Pcgf5*^{flox} allele. The *Pcgf5*-KO allele was generated by deleting the 2nd exon of *Pcgf5* by crossing mice carrying *Pcgf5*^{flox} with CAG-Cre mouse strain. The *Pcgf5* mutant line was maintained as heterozygotes and KO mice were obtained by mating *Pcgf5*$^{+/-}$ female with *Pcgf5*$^{+/-}$ male. Genomic positions of PCR primers (P1 and P2) used for genotyping are indicated by red arrows. (E) PCR analysis to distinguish the wild type (WT), *Pcgf5*$^{+/-}$ (WT/KO) and *Pcgf5*$^{-/-}$ (KO).